Acta Polytechnica CTU Proceedings **40**:69–75, 2023
https://doi.org/10.14311/APP.2023.40.0069

Published by the Czech Technical University in Prague

EFFECT OF ELECTRIC CURRENT ON POROSITY OF CONCRETE

Daniel Ňachaj[a,*], Jiří Němeček [1,a], Milan Kouřil[b], Martin Keppert[c], Jiří Němeček [2,a]

[a] *Czech Technical University in Prague, Faculty of Civil Engineering, Department of Mechanics, Thákurova 7, 166 29 Prague 6, Czech Republic*

[b] *University of Chemistry and Technology, Department of Metals and Corrosion Engineering, Technická 5, 166 28 Prague 6, Czech Republic*

[c] *Czech Technical University in Prague, Faculty of Civil Engineering, Department of Material Engineering and Chemistry, Thákurova 7, 166 29 Prague 6, Czech Republic*

[*] corresponding author: nachadan@fsv.cvut.cz

Abstract. The paper describes the influence of electric current on the porosity of concrete samples after electrically accelerated tests and other electrokinetic treatments. Three different concrete mixtures consisting of CEM I 42.5R, CEM II / A-M(S-LL) 42.5R, and CEM I 42.5R with 10 % replacement of cement by microsilica were examined. Direct current (DC) test was performed on fully saturated samples. The samples were loaded with a constant voltage of 20 V for 24 hours in chambers filled with NaOH solution. The changes in porosity were examined using mercury intrusion porosimetry (MIP), scanning electron microscopy (SEM), and open porosity (OP). The results of open porosity indicate an increase in porosity for all mixtures measurements of ∼0.6 %–2 % for treated samples. The MIP showed increase of volume of pores with radius smaller than 0.01 µm after DC test. According to X-ray diffraction (XRD) and Thermogravimetric analysis (TGA) there was ∼2 % less calcite after DC test.

Keywords: Electricity, MIP, concrete, porosity, image analysis, microstructure.

1. Introduction

Concrete is a composite material composed of fine and coarse aggregate bonded together with a cement matrix. It is the most used building material in the world. Its advantage is high compressive strength, which is approximately ten times greater than tensile strength. Due to this characteristic, reinforced concrete has been invented. The most common and cheapest rebar is steel reinforcement, which is highly susceptible to corrosion when exposed to aggressive environment. Due to this unwanted characteristic, the durability of concretes can be considerably reduced [1, 2].

Reinforcement corrosion is influenced by the presence of deicing salts transported through the microstructure and cracks of damaged concrete towards reinforcement. The corrosion of steel reduces the cross-section of the reinforcement, which leads to the loss of its load-bearing capacity. Chloride-induced corrosion of the reinforcement is one of the main causes of degradation of structural concrete and also a contributor to the cost of rehabilitation of concrete structures. In order to prevent reinforcement corrosion and reduce chloride/salt penetration, the concrete cover is usually increased, or the permeability of concrete is decreased [2, 3]. Also, non-destructive healing methods based on electromigration have been proposed to eliminate corrosion [4]. For example, a method of electrochemical chloride extraction (ECE) has been successfully used to reduce chloride attacks in concrete bridges [5].

Electrochemical remediation techniques are based on the accelerated transport of charged particles or ions inside the pore structure under the influence of an electric field. Electrokinetic treatment with nanoparticles has recently been introduced to improve the concrete microstructure and increase durability by blocking concrete pores [6].

In order to improve the properties of concrete mixtures, the permeability of the concrete to ions is often determined as quality control. Chloride diffusion measurements require a long time to determine steady-state conditions. Therefore, a direct current potential is usually used to accelerate ion migration. One of the standardized electric tests is according to ASTM C1202 standard [7] also called Rapid Chloride Permeability Test (RCPT) which is used to determine concrete chloride permeability [8–10].

Electrokinetic techniques are applied in many fields allowing the manipulation of material properties. These techniques are used in the concrete industry, primarily to mitigate corrosion of reinforcement but also to modify the microstructure of cement-based systems, thereby improving their long-term properties. Electrokinetic treatment is used to mitigate corrosion and is proposed for microstructural refinement / durability enhancement, crack healing, chemical attack recovery, and reinforcement-concrete bond enhancement [6].

[1] Ph.D. at Czech Technical University in Prague, Orcid: 0000-0002-5635-695X.

[2] Professor at Czech Technical University in Prague, Orcid: 0000-0002-3565-8182.

It was found that the electric current has some side effects and increases the porosity [11, 12]. Thus, it is important to investigate the effect of electric current on the microstructure of the cement matrix, as this has not been sufficiently investigated so far. Therefore, this paper focuses on the influence of the electric current on the porosity of different types of concrete.

2. Experimental methods

2.1. Direct Current test

There are several standardized accelerated tests for chloride penetration to concrete. One of them, the Rapid Chloride Permeability Test (RCPT) measures the electric charge transferred through concretes from which it is possible to determine their resistance to chloride ion penetration on various mixtures. The test is carried out by monitoring the amount of electric current that passes through the concrete samples in a specified time. The standard test according to AST C1202 consist of cylindrical 50 mm thick slices with a diameter of 100 m. The concrete samples are exposed to a potential difference of 60 V direct current for 6 hours, where electric current passing through samples is monitored [7]. In the chambers there is the negative pole in 0.52 N NaCl solution and positive pole in 0.30 N NaOH solution which are in contact with sample's base. The Direct Current (DC) test used in this work was inspired by the RCPT test with a modified setting. In the DC test, the voltage was set to 20 V with the duration of 24 hours to better simulate settings used for chloride extraction on real structures. Also, the NaOH with 0.3 M concentration was present in both chambers. No chlorides were present in the DC test, see Figure 1.

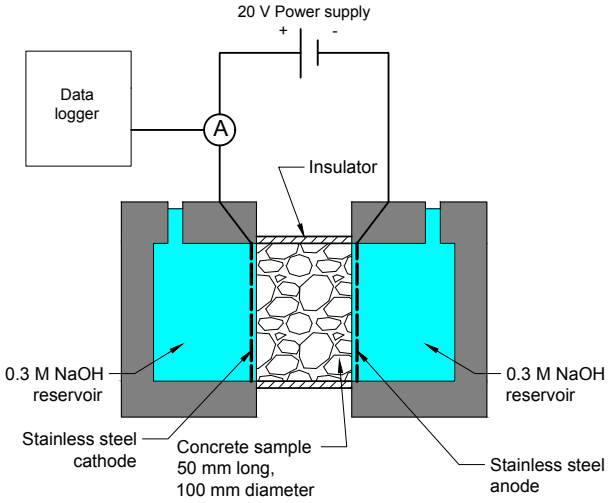

Figure 1. Scheme of DC test.

2.2. Open Porosity

The Open Porosity (OP) measures the physically bound water in the pores. Its weight is needed to determine the total open porosity. The open porosity, ϕ_{OP} is then calculated according to the equation:

$$\phi_{\mathrm{OP}} = \frac{V_{\mathrm{w}}}{V_{\mathrm{s}}} = \frac{m_{\mathrm{w}} - m_{\mathrm{d}}}{V_{\mathrm{s}}.\rho_{\mathrm{w}}}, \qquad (1)$$

where

V_{w} is a volume of the water,

V_{s} is a volume of the concrete sample,

m_{w} is a weight of fully saturated sample,

m_{d} is a weight of dried sample,

ρ_{w} is a density of water assumed as 998 kg/m^3 at 20 °C.

2.3. Mercury Intrusion Porosimetry

Several methods are generally used to measure the porous structure of concrete, such as the optical methods, mercury intrusion porosimetry (MIP), gas absorption, proton nuclear magnetic resonance (1H-NMR), and X-ray microtomography [13]. MIP has been used for many years to investigate the porous structure of cement-based materials. MIP also provides information about the connectivity of the pores [14]. Measurement of porosity by mercury intrusion provides an extensive range of measurable pore sizes from 4 nm to 500 µm. However, it is important to note that mercury intrusion porosimetry only measures the open pores [15].

2.4. Image Analysis

Image analysis (IA) is used for the observation of cement paste phases. The observed parameters are e.g. the size of the phases, their representation, and shape. Images are made in a gray range (0–255) of colors, and the colors of pixels vary according to the density of the physical element. The darker colored pixel in the Scanning Electron Microscope (SEM)-BackScattered Electrons (BSE) image represents elements with a lower proton number, while the lighter colored pixel, on the other hand, represents areas with elements with a higher proton number [16].

During the image analysis, adequate gray-level threshold extraction is necessary. Otsu method can perform automatic image thresholding, whose algorithm in its simplest form returns a single intensity threshold that separates pixels into two classes [17].

2.5. X-ray Diffraction

X-ray diffraction (XRD) is a technique that provides chemical information for elemental analysis as well as for phase analysis. Samples to be analyzed using XRD must be crystalline as concrete samples partly are [18]. XRD analysis is used to show cement microstructure's phases such as Portlandite, Calcite, AFm, and AFt, where the microstructure changes of a cement matrix are expected during current application [19].

2.6. Thermogravimetric analysis

Thermogravimetric analysis (TGA) is a method that captures the change in sample weight as a function

Label	CEM I 42.5R [kg]	CEM II 42.5R [kg]	MS [kg]	Water [kg]	sand 0–4 mm [kg]	agg 4–8 mm [kg]	agg 8–16 mm [kg]
cA	261.8	0	0	210.2	1150.0	290.9	581.8
cB	0	261.8	0	210.2	1150.0	290.9	581.8
cC	235.6	0	26.2	210.2	1150.0	290.9	581.8

Legend: aggregate (agg), microsilica (MS).

TABLE 1. Samples labeling with the specific weights of the additives in kg.

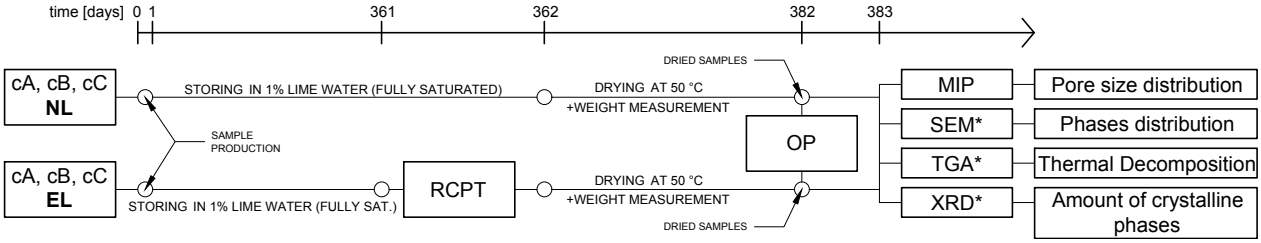

FIGURE 2. Experimental flow. Note: *for cA samples only.

of temperature. This method monitors the weight of a sample of the substance under investigation as its temperature changes. TGA characterizes and identifies phases from a complex cement matrix [20]. Similarly to XRD analysis, changes in the C-S-H phase, Portlandite, and calcite can be observed [19].

3. Experimental part

3.1. Experimental plan and sample preparation

Three types of concrete samples were produced, 2 samples of each type, each with a 0.8 water-binder (w/b) ratio and with aggregates of size 0-16 mm as it is shown in Table 1. The first sample (cA) was made of CEM I 42.5R, the second (cB) of CEM II / A-M(S-LL) 42.5R, and the third (cC) of CEM I 42.5R with 10 % cement replacement by microsilica. The concrete slurry was poured into cylindrical plastic ampules with a base diameter of 100 mm and a cylinder height of 250 mm. The following day, the hardened samples were demoulded, cut into 50 mm thick slices, and stored in 1 % lime water solution. From each type of concrete one sample was loaded with electric current, following the OP measurement. Later, the pieces necessary for further experiments were taken from all the samples. The MIP was performed on every type of the sample. SEM, TGA, XRD was only performed on the cA samples, because of capacity and time reasons. The overall experimental flow is also shown in Figure 2.

3.2. DC test

One year saturated samples were exposed to a constant voltage of 20 V for 24 hours. The scheme of the experiment is shown in Figure 1. The stainless steel electrodes were placed in two chambers filled with 0.3 M NaOH solution. The concrete sample was placed between both chambers to create the conductive path. The electric current is conducted through continuously connected pores filled with pore solution. The samples loaded by the electric current are labeled EL, and samples not loaded by the electric current are marked as NL. During the DC test the voltage was set as constant and the current was measured. The charge, Q, can then be expressed by formula:

$$Q = \int I(t)dt, \tag{2}$$

where

I is the the current,

t is the time.

3.3. Open Porosity

After DC test OP was measured. Fully saturated samples were placed in an oven at 50 °C, and the sample's mass was sequentially measured to detect the water loss. Samples were considered dried if the daily water loss ratio to the fully saturated sample was less than 0.1 % for at least 2 consecutive days. The period for which the samples have usually dried is approximately 20 days.

Following the open porosity measurement the dried samples were broken to the pieces for another analysis.

3.4. MIP

MIP was performed on samples weighing ∼1.5 g. The measurements were performed on an AutoPore IV 9500 instrument for pore sizes ranging from 0.0015 µm to 130 µm.

3.5. Image Analysis

The samples fragment were cast with epoxy resin into cylindrical molds, then cut into 6 m slices and polished according to the procedure described in [21]. Prepared samples were observed by SEM Phenom XL.

10 BSE images were performed on each sample on the spots carefully chosen in the cement matrix. Thus, magnification varied from 1350× to 1600× to avoid aggregates. Totaly covering area 0.5 mm^2, which is sufficient for statistical analysis [21].

3.6. XRD and TGA

Both XRD and TGA experiments were performed only on cA samples for capacity and time reasons. Simultaneous thermal analysis (STA), consisting of differential scanning calorimetry (DSC) and thermogravimetry (TG), was carried out using a Labsys EVO TG/DSC from Setaram Inc. Experiments were done in the temperature range from 30 °C to 1000 °C with a heating rate of 5 °C/min. An argon atmosphere with a flow rate of 40 ml/min was set during the measurements. XRD was performed using the powder diffraction technique using X-ray. It was done by PANalytical Aeris machine with Bragg-Brentano arrangement.

4. Results and discussion

4.1. Results of DC test

Samples cB and cC show the expected trend of relatively constant electric current. The electric current waveform for sample cC is fluctuating and it is also lower than for sample cB. However, the trend is the same for both samples. The current of sample cA is increasing at the beginning of the test, followed by an constant current progression followed by a current drop after 16 hours of the test. Typical curves are shown in Figure 3.

The results of the calculated total transferred charges are summarized in Table 2. The smallest charge was measured for the cC sample that could be assigned to a higher sample resistance due to microsilica supplement. On the other side cA sample without admixture showed the highest charge suggesting the lowest resistance and highest porosity compared to other samples. This could be due to the fact that the cA sample contains more large pores through which more electric current passes, see Figure 4.

Label	**cA** Q [C]	**cB** Q [C]	**cC** Q [C]
-EL	3967	3285	2996

Table 2. Total charge measured during DC test.

4.2. Results of Open Porosity

The results of open porosity indicate the impact of electric current on the porosity of different concrete mixtures. All three mixtures show an increase in porosity after the DC test, see Table 3. The highest increase of open porosity by ∼2 % was found for the cA-EL sample. The mixtures with admixtures (cB and cC) exhibited a minor increase in open porosity below 1 %. The larger change for the cA sample

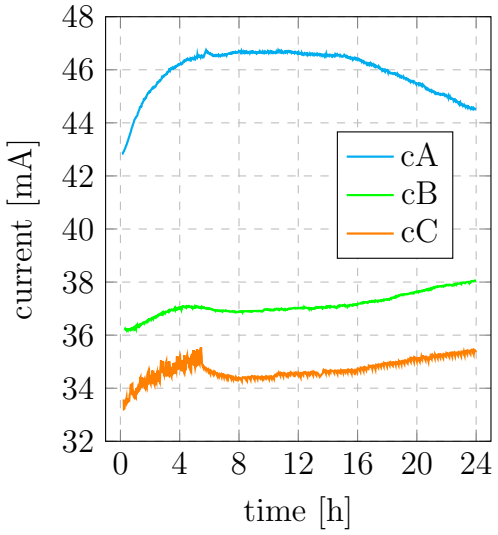

Figure 3. Change of the electric current over time during DC test.

could be due to a different admixture and so different microstructure. However, the OP can only measure free-water that is evaporated from the sample.

Label	**cA** ϕ_{OP} [%]	**cB** ϕ_{OP} [%]	**cC** ϕ_{OP} [%]
-NL	12.22	12.70	11.47
-EL	14.27	13.34	12.30
Change	+2.05	+0.64	+0.83

Table 3. Results of open porosity.

4.3. Results of MIP

Results of total porosity measured by MIP are summarized in Table 4. Similarly to open porosity, MIP did not show significant changes between the samples. The results for cA sample agree with those one obtained from OP. However, a decrease in porosity was found for cB and cC samples after the DC test.

Label	**cA** [%]	**cB** [%]	**cC** [%]
-NL	15.69	16.25	16.21
-EL	16.62	14.47	15.89
Change	+0.93	−1.78	−0.32

Table 4. Results of porosity determined by MIP.

The pore size distribution curves measured by MIP are shown in Figure 5 for individual samples loaded and non-loaded by the current. It is possible to observe a shift of the main porosity peak into the smaller values after the DC for all three mixtures. That is in agreement with the study of Susanto et al. [11], where a similar shift was observable for mortar samples.

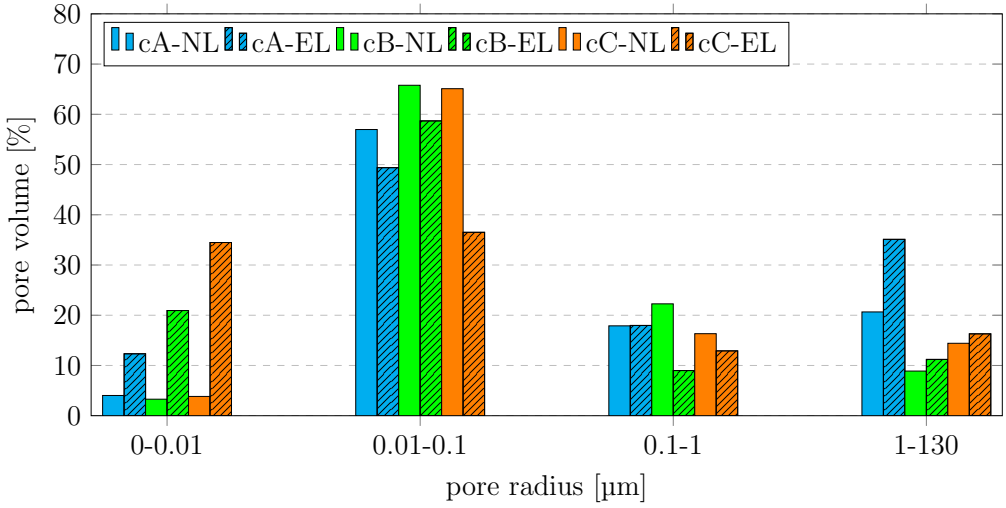

FIGURE 4. Pores volume changes in the different size ranges of samples loaded and non-loaded by the electric current.

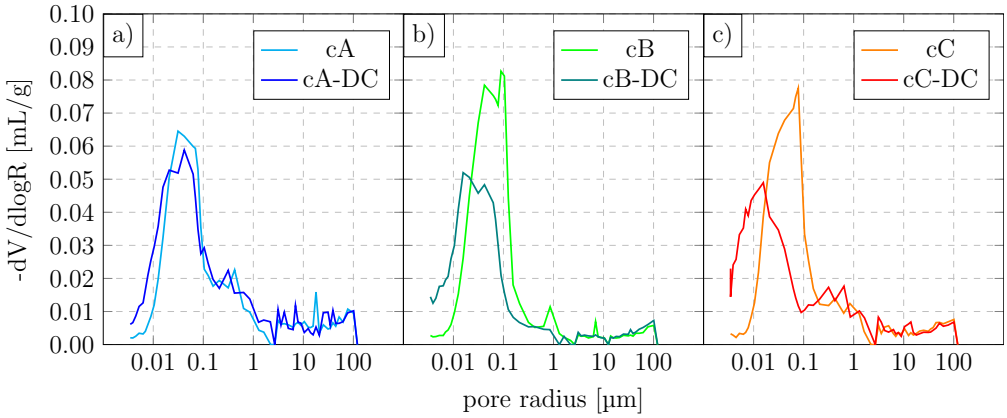

FIGURE 5. Pore size distribution curves of samples loaded and non-loaded by the electric current.

Figure 4 displays the changes in pore distribution in different intervals. There is evident increase of pore volume with a radius smaller than 0.01 µm after the current test. The increase is accompanied by the decrease of pores volume in the range (0.01–0.1) µm. The pores of a radius higher than 0.1 µm do not show any significant changes except for the cA sample where the increase of pores in the interval 1 µm–130 µm by ∼14 % takes place. The change in the distribution of the volume of pores is obvious, as are the trends. This means that after passing through an electric current, the distribution of the pores volume representation according to its radius changes, see Figure 4.

4.4. Results of Image Analysis

Image analysis was applied to SEM-BSE images of the cA sample. Due to similar pixel intensity, only two phases were separated. The first phase was composed primarily of pores, but cracks and scratches were also present, as visible in Figure 6. The second phase contains the rest of the phases, mainly hydration products, residual clinker, or small aggregates. The results of IA and phase volume fraction are shown in Table 5, indicating a growth of the phase representing pores by 1.78 % for samples loaded with electric current.

Label	Pores/cracks [%]	Other phases [%]
cA-NL	2.82 ±0.99	97.18 ±0.99
cA-EL	4.60 ±2.18	95.40 ±2.18
Change	+1.78 ±1.59	−1.78 ±1.59

TABLE 5. Volume fraction of phases obtained from image analysis.

4.5. Results of TGA

TG and DSC analysis revealed three distinct thermal decomposition processes. Firstly, the physically bound (PB) water and water bound chemically in C-S-H hydrates evolved between the ambient temperature and ∼250 °C. Portlandite $Ca(OH)_2$ decomposes between 450 and 500 °C and finally $CaCO_3$ polymorphs (Calcite, amorphous $CaCO_3$) between 610 and 800 °C. The tangential method [22] determined the content of Portlandite and $CaCO_3$ polymorphs. The content of Portlandite in both samples is equal; the sample cA-NL contains 0.71 % more hydration products as well as 1.9 % more calcite, see Table 6. This could mean, that due to the electric current

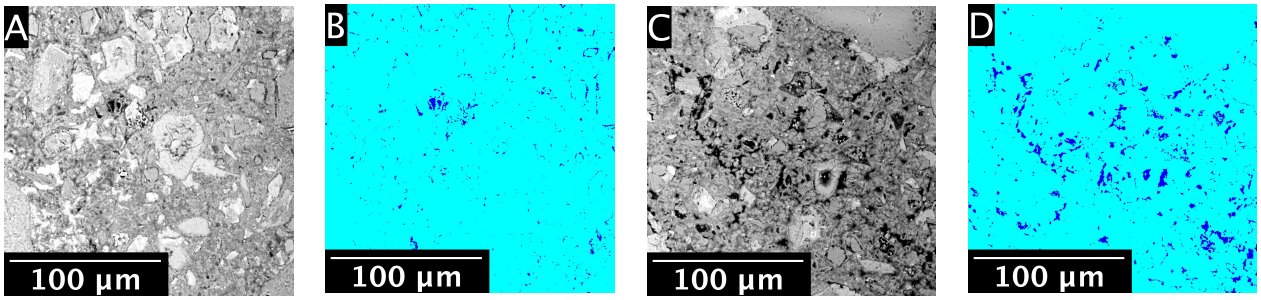

(A). SEM-BSE image: cA-NL. (B). IA with phase separation: cA-NL. (C). SEM-BSE image: cA-EL. (D). IA with phase separation: cA-EL.

Figure 6. Typical SEM-BSE image of samples cA-NL, cA-EL. Example of IA with phase separation: pores/cracks (blue), hydration products, residual clinker (cyan) of samples cA-NL, cA-EL.

treatment the calcite is leaching out of the sample.

Label	PB water, C-S-H, gypsum [%]	Portlandite* [%]	Calcite* [%]
cA-NL	6.88	6.52	5.59
cA-EL	6.17	6.52	3.69

Legend: *tangent method [22].

Table 6. Content of thermally-decomposed components (% by mass) where PB means physically bound.

4.6. Results of XRD

The phase composition obtained by XRD is presented in Table 7. The system is very complicated due to the presence of mixed aggregates containing not only quartz but also many feldspar minerals (anorthite, oligoclase, albite, orthoclase), which are very similar and difficult to distinguish. It must also be kept in mind that concrete contains a lot of C-S-H, which are amorphous and hence not indicated by XRD. Moreover, the concrete samples with coarse aggregates pose a risk of homogeneity and representativeness. Thus these results should be considered just as an indication. The content of calcite and portlandite seems to be 2 % higher for both of them in cA-NL, which agrees with thermal analysis.

Phase	cA-NL [%]	cA-EL [%]
Portlandite	9	7
Calcite	6	4
AFt	2	1
AFm	3	4

Table 7. The phase composition in % obtained from XRD.

4.7. Mutual comparisons

The sample cA exhibits an increase in total porosity for samples loaded by current by all three measurement methods (OP +2.05 %, MIP +0.93 %, IA +1.78 %). The reason might be given by microstructure changes and dissolution of Portlandite, calcite, and AFt phases. That was confirmed by XRD/TGA analyses and is with the agreement of study of Ottosen et al. [19].

The results of the cB and cC samples are a bit different. There was an increase in open porosity, which was not confirmed by MIP. The reason might be given by the different pore size measuring ranges between those two techniques where MIP did not capture the change in large pores for cB and cC samples, contrary to the cA sample. Despite this, the transition to smaller pores is even more pronounced for cB and cC samples as visible in Figures 4, 5.

Overall, the DC test shows that the most of the electric current has passed through the cA sample which is in agreement with the OP and MIP showing the biggest increase of porosity after the treatment.

5. Conclusions

This paper describes changes in concrete porosity after the loading by direct current. The porosity was evaluated by three porosity measurement techniques: open porosity, mercury intrusion porosimetry, and image analysis of SEM-BSE images. The most important conclusions are summarized in the following points:

- The influence of the electric current on the porosity of individual samples is different for various concrete mixtures depending on their composition and microstructure.
- Based on the open porosity results. One day treatment with electric current affects the porosity of concrete mixtures and increases it by 0.64 % to 2.05 %, depending on the mixture.
- The increase of porosity for concrete sample made of ordinary Portland cement takes place at the expense of other phases like Portlandite, calcite, or AFm.
- Based on the MIP observation, the pores volume in the range (0.01–0.1) µm is decreased and in the

range (0–0.01) µm is increased after the DC test. The difference is most pronounced for the sample modified with microsilica.

Acknowledgements

Financial support of the Czech Science Foundation (project No. 21-11965S) and the Grant Agency of the Czech Technical University in Prague (SGS22/088/OHK1/2T/11) are gratefully acknowledged.

References

[1] C. R. Gagg. Cement and concrete as an engineering material: An historic appraisal and case study analysis. *Engineering Failure Analysis* **40**:114–140, 2014. https://doi.org/10.1016/j.engfailanal.2014.02.004

[2] R. Loser, B. Lothenbach, A. Leemann, M. Tuchschmid. Chloride resistance of concrete and its binding capacity – comparison between experimental results and thermodynamic modeling. *Cement and Concrete Composites* **32**(1):34–42, 2010. https://doi.org/10.1016/j.cemconcomp.2009.08.001

[3] A. Guettala, A. Abibsi. Corrosion degradation and repair of a concrete bridge. *Materials and Structures/Materiaux et Constructions* **39**(288):471–478, 2006. https://doi.org/10.1617/s11527-005-9046-z

[4] J. Němeček, L. Li, Y. Xi. Electrokinetic nanoparticle injection for remediating leaks in oil well cement. *Construction and Building Materials* **156**:63–72, 2017. https://doi.org/10.1016/j.conbuildmat.2017.08.152

[5] J. Němeček, J. Kruis, T. Koudelka, T. Krejčí. Simulation of chloride migration in reinforced concrete. *Applied Mathematics and Computation* **319**:575–585, 2018. https://doi.org/10.1016/j.amc.2017.07.029

[6] N. Jafariesfad, M. Geiker, S. Sangesland, et al. Electrokinetics application in concrete and well construction. In *International Conference on Offshore Mechanics and Arctic Engineering*, vol. Volume 11: Petroleum Technology. 2020. V011T11A031. https://doi.org/10.1115/OMAE2020-18275

[7] ASTM. Standard test method for electrical indication of concrete's ability to resist chloride ion penetration, 2012. C1202–18.

[8] K.-S. Huang, C.-C. Yang. Using RCPT determine the migration coefficient to assess the durability of concrete. *Construction and Building Materials* **167**:822–830, 2018. https://doi.org/10.1016/j.conbuildmat.2018.02.109

[9] S. Safarzadegan Gilan, H. Bahrami Jovein, A. A. Ramezanianpour. Hybrid support vector regression – Particle swarm optimization for prediction of compressive strength and RCPT of concretes containing metakaolin. *Construction and Building Materials* **34**:321–329, 2012. https://doi.org/10.1016/j.conbuildmat.2012.02.038

[10] M. Jemimah Carmichael, G. Prince Arulraj. Rapid chloride permeability test on concrete with nano materials. *International Journal of Engineering and Advanced Technology (IJEAT)* **8**(3S), 2019. [2022-08-18]. https://www.ijeat.org/wp-content/uploads/papers/v8i3S/C10210283S19.pdf

[11] A. Susanto, D. A. Koleva, K. van Breugel, K. van Beek. Stray current-induced development of cement-based microstructure in water-submerged, $Ca(OH)_2$-submerged and sealed conditions. *Journal of Advanced Concrete Technology* **15**(6):244–268, 2017. https://doi.org/10.3151/jact.15.244

[12] M. Siegwart, J. F. Lyness, B. J. McFarland. Change of pore size in concrete due to electrochemical chloride extraction and possible implications for the migration of ions. *Cement and Concrete Research* **33**(8):1211–1221, 2003. https://doi.org/10.1016/S0008-8846(03)00047-4

[13] A. Aili, I. Maruyama. Review of several experimental methods for characterization of micro-and nano-scale pores in cement-based material. *International Journal of Concrete Structures and Materials* **14**(1):55, 2020. https://doi.org/10.1186/s40069-020-00431-y

[14] A. B. Abell, K. L. Willis, D. A. Lange. Mercury intrusion porosimetry and image analysis of cement-based materials. *Journal of Colloid and Interface Science* **211**(1):39–44, 1999. https://doi.org/10.1006/jcis.1998.5986

[15] C. Voigt, J. Hubálková, H. Giesche, C. G. Aneziris. Intrusion and extrusion mercury porosimetry measurements at Al_2O_3–C – Influence of measuring parameter. *Microporous and Mesoporous Materials* **299**:110125, 2020. https://doi.org/10.1016/j.micromeso.2020.110125

[16] A. Luis, L. Deng, L. Shao, H. A. Li. Triaxial behaviour and image analysis of Edmonton clay treated with cement and fly ash. *Construction and Building Materials* **197**:208–219, 2019. https://doi.org/10.1016/j.conbuildmat.2018.11.222

[17] N. Otsu. A threshold selection method from gray-level histograms. *IEEE transactions on systems, man, and cybernetics* **9**(1):62–66, 1979. https://doi.org/10.1109/TSMC.1979.4310076

[18] S. Nasrazadani, S. Hassani. Chapter 2 - Modern analytical techniques in failure analysis of aerospace, chemical, and oil and gas industries. In A. S. H. Makhlouf, M. Aliofkhazraei (eds.), *Handbook of Materials Failure Analysis with Case Studies from the Oil and Gas Industry*, pp. 39–54. Butterworth-Heinemann, 2016. https://doi.org/10.1016/B978-0-08-100117-2.00010-8

[19] L. M. Ottosen, I. V. Christensen, I. Rörig-Dalgård, et al. Utilization of electromigration in civil and environmental engineering–Processes, transport rates and matrix changes. *Journal of Environmental Science and Health, Part A* **43**(8):795–809, 2008. https://doi.org/10.1080/10934520801973949

[20] A. W. Coats, J. P. Redfern. Thermogravimetric analysis. A review. *Analyst* **88**:906–924, 1963. https://doi.org/10.1039/AN9638800906

[21] J. Němeček, J. Lukeš, J. Němeček. High-speed mechanical mapping of blended cement pastes and its comparison with standard modes of nanoindentation. *Materials Today Communications* **23**:100806, 2020. https://doi.org/10.1016/j.mtcomm.2019.100806

[22] K. Scrivener, R. Snellings, B. Lothenbach, et al. *A practical guide to microstructural analysis of cementitious materials*, vol. 540. CRC Press Boca Raton, FL, USA, 2016.